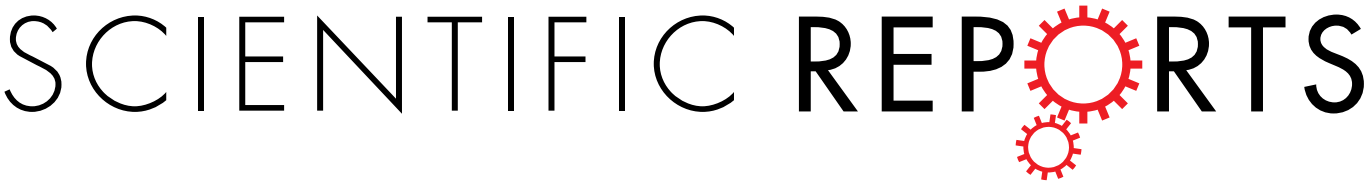

OPEN

Effects of light on quantum phases and topological properties of two-dimensional Metal-organic frameworks

Received: 28 October 2016
Accepted: 20 December 2016
Published: 30 January 2017

Yunhua Wang[1,2], Yulan Liu[3] & Biao Wang[1,2]

Periodically driven nontrivial quantum states open another door to engineer topological phases in solid systems by light. Here we show, based on the Floquet-Bloch theory, that the on-resonant linearly and circularly polarized infrared light brings in the exotic Floquet quantum spin Hall state and half-metal in two-dimensional Metal-organic frameworks (2D MOFs) because of the unbroken and broken time-reversal symmetry, respectively. We also observe that the off-resonant light triggers topological quantum phase transitions and induces semimetals with pseudospin-1 Dirac-Weyl fermions via the photon-dressed topological band structures of 2D MOFs. This work paves a way to design light-controlled spintronics and optoelectronics based on 2D MOFs.

Once discovered in materials, quantum states, with extra degrees of freedom, unconventional conical bands or nontrivial topological features, could yield entirely new physics and device paradigms in nanoelectronics and information technology. The first example is the half-metallic state with 100% spin polarization near the Fermi energy, where the spin degree of freedom can be used as information carriers in spintronics[1]. The second example is the semimetallic state in graphene with linear electronic band dispersion associated with the Dirac physics[2]. As a counterpart of the electronic spin, the extra valley degree of freedom used as information carriers in graphene, silicene or monolayer transition metal dichalcogenides could lead to the exotic valleytronics[3,4]. The third example is the topological insulators (TIs), where fully spin-polarized currents carried by the robust conducting edge or surface states inside the insulating bulk gap allow TIs for applications in spintronics and quantum computation[5,6]. In addition, more exotic quantum states have also been explored recently, such as Weyl semimetals[7–9], axion insulators and three-dimensional Dirac semimetals[10,11]. Besides searching for materials with these exotic quantum states, engineering these states in condensed matter or nanostructures by external fields also has aroused tremendous attention during the past few years.

Via photon-dressed band structures and properties in Floquet-Bloch picture, light-matter interaction not only offers novel experimental and theoretical platforms for engineering Floquet topological insulating phases[12–30] and semimetallic phases[31–36] in solid systems, but also sparks the same interest in photonic crystals and optical lattices[37–42]. These Floquet quantum states not only display similar behaviours as their counterparts in static system but also exhibit additional features, which require the extension of the classifications[13,43–47] and are directly manifested by their unique nonequilibrium transport properties[16–18,48–53]. In general, the Floquet-Bloch theory, which describes the interaction of light with Bloch states in solids, can be divided into two classes in view of two distinct physical mechanisms. The first is based on the zeroth static Floquet Hamiltonian in the off-resonant regime, where the driving frequency ω is larger than the bandwidth Λ of the undriven system. In this case, the real absorption and emission for a photon with frequency ω between the uncoupled Floquet sidebands are unlikely, but the virtual photon absorption and emission[17] can incorporate with the Bloch electrons and renormalize the electronic structures. The second is governed by the truncated Floquet Hamiltonian in the on-resonant regime ($\omega < \Lambda$), where the overlapped Floquet sidebands and the photon resonances are responsible for these exotic Floquet quantum states[15,20,24,43].

[1]Sino-French Institute of Nuclear Engineering and Technology, Sun Yat-sen University, Zhuhai 519082, China. [2]State Key Laboratory of Optoelectronic Materials and Technologies, Sun Yat-sen University, Guangzhou 510275, China. [3]School of Engineering, Sun Yat-sen University, Guangzhou 510275, China. Correspondence and requests for materials should be addressed to Y.W. (email: wangyh49@mail.sysu.edu.cn) or B.W. (email: wangbiao@mail.sysu.edu.cn)

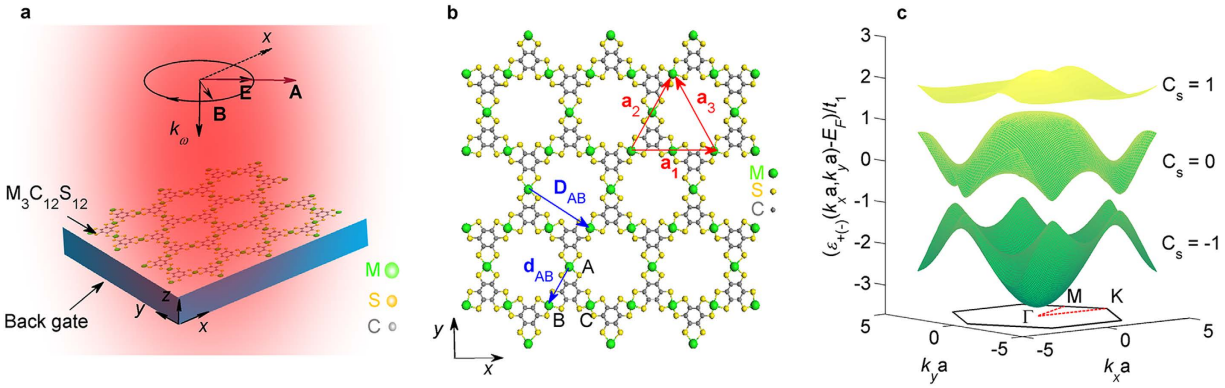

Figure 1. Photon-dressed topological band structures of $M_3C_{12}S_{12}$. (**a**) Schematic of light-irradiated $M_3C_{12}S_{12}$ on a back gate controlling the Fermi energy E_F. Infrared light with the incident wave vector k_ω travels along the negative z axis (perpendicular to the $M_3C_{12}S_{12}$ plane) and induces the time-dependent vector potential $\mathbf{A}(t) = (A_x \sin(\omega t), A_y \sin(\omega t + \phi), 0)$ with the frequency ω. (**b**) 2D kagome lattice of $M_3C_{12}S_{12}$. Here, $\mathbf{a}_1 = (1, 0)a$, $\mathbf{a}_2 = (1/2, \sqrt{3}/2)a$, and $\mathbf{a}_3 = \mathbf{a}_2 - \mathbf{a}_1$ are the lattice vectors with the lattice constant a, $\mathbf{d}_{ij}$ ($i, j =$ A, B or C, *i.e.*, the sublattices) is the nearest-neighbor vector, and $\mathbf{D}_{ij}$ is the next-nearest-neighbor vector. (**c**) The photon-dressed topological band structures of $M_3C_{12}S_{12}$ with a group of spin chern numbers (−1, 0, 1) from bottom up, for $A_x a = 1.5$, $A_y a = 1.5$, $\phi = 0$, and $\lambda_1 = 0.14 t_1$.

In this work, we focus on the coherent interaction of light with the recently discovered two-dimensional Metal-organic frameworks (2D MOFs)[54–57], in both of the off-resonant and on-resonant Floquet-Bloch pictures. Owing to the numerous combinations of different metal ions and organic ligands, 2D MOFs have various chemical structures and versatile physical and chemical functionalities[58], such as topological electronic properties[59–66], Dirac semimetals[67], half-metallicity[68] and chemiresistive response[69]. The dominant nearest-neighbor hopping ($0.01\,\text{eV} < t_1 < 0.1\,\text{eV}$)[59–68] in 2D MOFs is much less than that in graphene ($t_1 \sim 2.8\,\text{eV}$)[2], and hence only needs the coupling light with a lower frequency ($\omega < 1.2 \times 10^{14}\,\text{Hz}$) in infrared, which is experimentally accessible[19]. Consequently, the infrared sensitivity opens a door to engineer quantum states in 2D MOFs by light. Herein, we report the effects of infrared light on the quantum phases and topological properties of $M_3C_{12}S_{12}$ (M is a metal ion, such as Ni, Cu, Pt, Au and others)[58], a kind of 2D MOFs with kagome lattice (Fig. 1a and b), within the framework of the Floquet-Bloch physics. It is shown that photoinduced quantum phases in $M_3C_{12}S_{12}$ can be attributed to the Floquet-Peierls (FP) substitutions, which allow the effective lattices to be engineered through the renormalized hoppings as well as the spin-orbit couplings (SOC) and permit the Floquet quantum phases to be customized by the photon-dressed band structures and topological properties. Under the off-resonant light irradiation, the nonzero FP substitutions maintain the kagome lattice but with modified strengths, which can reverse three energy bands of $M_3C_{12}S_{12}$ with different spin chern numbers and hence trigger a topological quantum phase transition. Single zero FP substitution transforms the kagome lattice into the topologically equivalent Lieb lattice, which supports the semimetals with the Pseudospin-1 Dirac-Weyl fermions. Under the on-resonant light irradiation, the circularly polarized light with frequency ($\Lambda/2 < \omega < \Lambda$) induces robust Floquet half-metal by virtue of the broken time-reversal symmetry, but the linearly polarized light with lower frequency ($t_1 < \omega < \Lambda/2$) brings in the exotic Floquet quantum spin Hall state with the gapless helical edge states protected by the time-reversal symmetry. These results demonstrate that Dirac semimetals, Floquet half-metal and Floquet topological insulating states can be engineered in the same 2D MOFs by tuning the driving parameters (frequency, amplitudes and polarization) of light, and therefore open a new way to design light-controlled spintronics and optoelectronics based on 2D MOFs.

Results

The zeroth static Floquet Hamiltonian. First, let us consider the effects of light on $M_3C_{12}S_{12}$ (Fig. 1a) in the off-resonant regime ($\omega > \Lambda$). In this case, the Floquet sidebands are uncoupled, and the photon-dressed band structures can be captured by the zeroth static Floquet Hamiltonian (see Methods in details)

$$\widetilde{H}_0 = E_0 \sum_{i\sigma} c_{i\sigma}^\dagger c_{i\sigma} - t_1 \sum_{\langle i,j\rangle \sigma} \widetilde{f}_{i,j}^{0,0}\, c_{i\sigma}^\dagger c_{j\sigma} + i\frac{8\lambda_1}{\sqrt{3}} \sum_{\langle i,j\rangle \alpha\beta} \widetilde{f}_{i,j}^{0,0}\, (\mathbf{d}_{kj} \times \mathbf{d}_{ik}) \cdot \mathbf{S}_{\alpha\beta} c_{i\alpha}^\dagger c_{j\beta}, \tag{1}$$

where $c_{i\alpha}^\dagger$ and $c_{i\alpha}$ are the creation/annihilation operators for an electron with the spin α on site $\mathbf{r}_i$, $\mathbf{S}$ is the spin Pauli matrix, and $\mathbf{d}_{kj}$ is the nearest-neighbor (denoted by $\langle i, j\rangle$) vector pointing from site $\mathbf{r}_j$ to $\mathbf{r}_k$ (see Fig. 1b). The constant on-site energy E_0 just shifts the whole energy spectrum, and hence is usually set to the zero energy[2]. The nearest-neighbor hopping energy t_1 and the intrinsic SOC strength λ_1 are modified by these FP substitutions

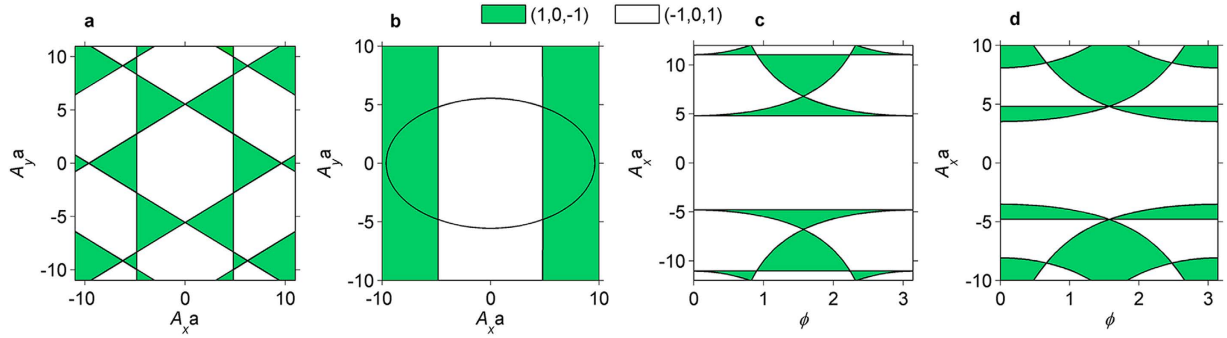

Figure 2. Phase diagram of light-irradiated $M_3C_{12}S_{12}$. (**a**) Phase diagram in the (A_x, A_y) plane for linearly polarized light ($\phi = 0$ or π). (**b**) Phase diagram in the (A_x, A_y) plane for circularly polarized light ($\phi = \pi/2$). (**c**,**d**) Phase diagrams in the (ϕ, A_x) plane for elliptically polarized light with $A_x = \sqrt{3}A_y$ and $A_x = A_y$, respectively.

$$\begin{aligned}
\widetilde{f}^{0,0}_{A,B} &= \widetilde{f}^{0,0}_{B,A} = J_0\left((a/4)\sqrt{A_x^2 + 3A_y^2 + 2\sqrt{3}A_xA_y\cos\phi}\right)\\
\widetilde{f}^{0,0}_{B,C} &= \widetilde{f}^{0,0}_{C,B} = J_0(\mathrm{a}|A_x|/2)\\
\widetilde{f}^{0,0}_{C,A} &= \widetilde{f}^{0,0}_{A,C} = J_0\left((a/4)\sqrt{A_x^2 + 3A_y^2 + 2\sqrt{3}A_xA_y\cos\phi}\right)
\end{aligned}, \tag{2}$$

where A_x and A_y are the amplitudes, ϕ is the phase difference reflecting the polarization of light, and $J_0(x)$ is the zeroth Bessel function of the first kind. The zeroth static Floquet Hamiltonian in equation (1) shows that the effects of the off-resonant light on the electronic properties of $M_3C_{12}S_{12}$ are decided by the FP substitutions, which allow us to design effective lattices by tuning the driving parameters (A_x, A_y and ϕ) of light: (1) If $\widetilde{f}^{0,0}_{i,j} \neq 0$, the hopping lattice of the irradiated $M_3C_{12}S_{12}$ remains the kagome lattice but with modified real hoppings that keep the time-reversal invariant, and hence $M_3C_{12}S_{12}$ maintains the topological insulating phases (Fig. 1c) because of the SOC; (2) If single FP substitution is zero, the hopping framework will become topologically equivalent to the Lieb lattice, which directly supports the semimetals with the pseudospin-1 Dirac-Weyl fermions near the Dirac points[70–74]; (3) If two or three FP substitutions are zero, the driven hopping lattice will be correspondingly equivalent to a quantum wire or some discrete lattice points such that 2D MOFs are always semimetals because of the touched conduction and valence bands with zero band gap.

Phase diagram and topological quantum phase transitions. We consider the phase diagrams of $M_3C_{12}S_{12}$ subjected to the light irradiation with linear, circular and elliptical (arbitrary) polarizations, respectively. In Fig. 2 we construct the phase diagrams in the (A_x, A_y) plane for linearly and circularly polarized light and in the (ϕ, A_x) plane for elliptically polarized light. In the case of the off-resonance that keeps the time-reversal symmetry, the topological insulating phases can still be characterized by a group of spin Chern numbers (C_s)[47,75,76] or Kane-Mele invariants[77] for the three distinct energy bands. From these phase diagrams, we can see that the off-resonant light induces two different topological insulating phases with the spin Chern numbers (-1, 0, 1) and (1, 0, -1), respectively. The topological phase transition occurs at the boundaries between the two different topological insulating phases, where the band gap is closed and the semimetal appears. In addition, the phase distributions are symmetrical owing to the symmetries of $\widetilde{f}^{0,0}_{i,j}$ with respect to the amplitudes A_x and A_y as well as the phase difference ϕ (see equation (2)). On the other hand, the edge state is a powerful tool to reveal the topological features of energy bands and search for the topological phase transitions, because of the bulk-edge correspondence. For TIs, fully spin-polarized gapless helical edge states protected by time-reversal symmetry are directly responsible for the spin Hall conductance (σ^s_{xy}). Therefore, the change of the spin Hall conductance can provide a signature of topological phase transitions. We calculate the edge state spectrum, the density of state and the spin Hall conductance for the two distinct TIs with $\lambda_1 = 0.14t_1$ (Fig. 3), on a cylindrical geometry, *i.e.*, a 34-unit-cell open boundary condition in the y direction and a periodic boundary condition in the x direction. As expected, the three bands of $M_3C_{12}S_{12}$ for the two different topological insulating phases are reversed, and a pair of robust spin-filtered gapless states inside each bulk gap leads to the contrary values of the quantized spin Hall conductance. As a result, the off-resonant light triggers the topological quantum phase transition between the two phases (-1, 0, 1) and (1, 0, -1).

Pseudospin-1 Dirac-Weyl fermions and flat band. In the above section, we concentrate on the topological insulating phases and phase transitions. Here we focus on the semimetals induced by the three cases: (*i*) $\widetilde{f}^{0,0}_{A,B} = 0$, $\widetilde{f}^{0,0}_{B,C} \neq 0$, and $\widetilde{f}^{0,0}_{A,C} \neq 0$, (*ii*) $\widetilde{f}^{0,0}_{A,B} \neq 0$, $\widetilde{f}^{0,0}_{B,C} = 0$, and $\widetilde{f}^{0,0}_{A,C} \neq 0$, (*iii*) $\widetilde{f}^{0,0}_{A,B} \neq 0$, $\widetilde{f}^{0,0}_{B,C} \neq 0$, and $\widetilde{f}^{0,0}_{A,C} = 0$. We elucidate the analytical expressions of photon-dressed energies $\varepsilon_{\pm}(\mathbf{k})$ and Hamiltonians $\widetilde{H}^{0,0}_{\pm}(\mathbf{k})$ for the semimetal phases in the three cases (see Supplementary Note 1). The obtained energy band structures of the

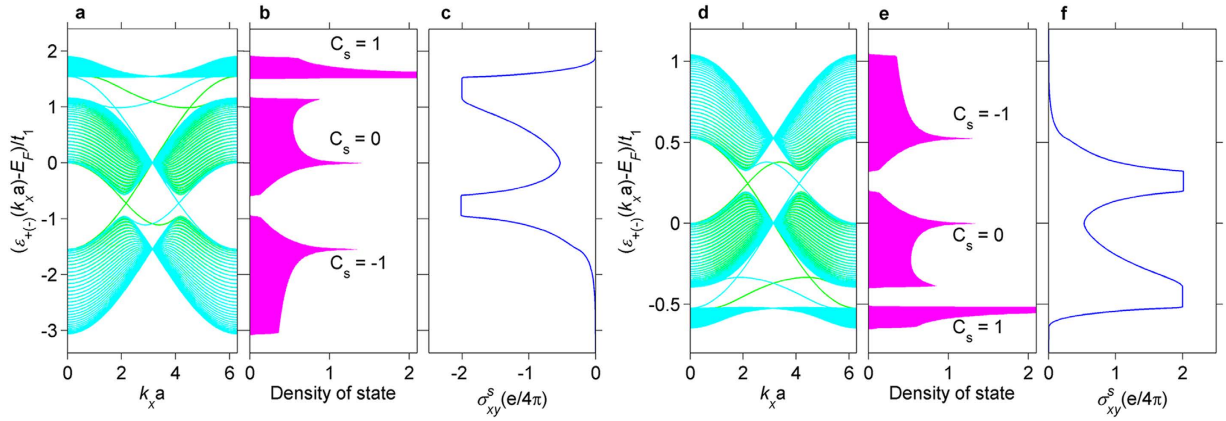

Figure 3. Edge state spectra of light-irradiated $M_3C_{12}S_{12}$ on a cylindrical geometry. For topological insulating phases (−1, 0, 1) with light parameters (A_xa = 2, A_ya = 2, and $\phi = \pi/2$) and (1, 0, −1) with light parameters (A_xa = 6, A_ya = 6, and $\phi = \pi/2$), respectively: The spin-up (green) and spin-down (cyan) edge state spectra in (**a,d**), the density of state in (**b,e**) and the spin Hall conductance in (**c,f**).

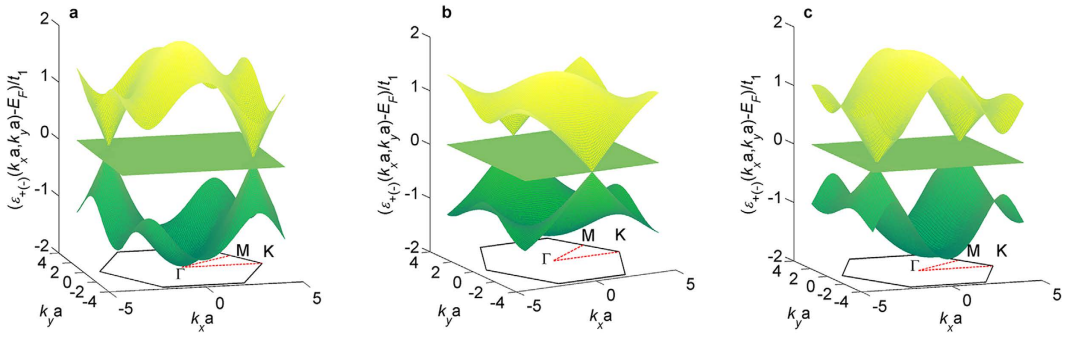

Figure 4. Light-induced semimetals with pseudospin-1 Dirac-Weyl fermions in $M_3C_{12}S_{12}$. (**a**) The photon-dressed band structure for case (*i*): $\tilde{f}^{0,0}_{A,B} = 0$, $\tilde{f}^{0,0}_{B,C} \neq 0$, and $\tilde{f}^{0,0}_{A,C} \neq 0$ with light parameters A_xa = 2, A_ya = 4.4, and $\phi = 0$. (**b**) The photon-dressed band structure for case (*ii*): $\tilde{f}^{0,0}_{A,B} \neq 0$, $\tilde{f}^{0,0}_{B,C} = 0$, and $\tilde{f}^{0,0}_{A,C} \neq 0$ with light parameters A_xa = 4.81, A_ya = 2, and $\phi = \pi/2$. (**c**) The photon-dressed band structure for case (*iii*): $\tilde{f}^{0,0}_{A,B} \neq 0$, $\tilde{f}^{0,0}_{B,C} \neq 0$, and $\tilde{f}^{0,0}_{A,C} = 0$ with light parameters A_xa = 2, A_ya = 6.71, and $\phi = 0$.

semimetals for the three cases with $\lambda_1 = 0.2t_1$ are shown in Fig. 4. Distinct from the light-induced extra Dirac cones at the surface of a topological insulator[21] or in graphene[23], two conical bands touch at the Dirac points, and an additional flat band exists. This band structure is the typical energy spectrum of the pseudospin-1 Dirac-Weyl fermions[70–74]. In this case, the spin degeneracy of the energy band is not lifted because of the time-reversal symmetry for the off-resonant light and the space-inversion symmetry of the light-engineered Lieb lattice in $M_3C_{12}S_{12}$ (Supplementary Note 1). The obtained effective Hamiltonians near the Dirac points (D_x, D_y) in the three cases can be rewritten as the general form of the pseudospin-1 Dirac-Weyl fermions: $\mathbf{H}_{eff,\pm} = v_x \mathbf{S}_{x,\pm} p_x + v_y \mathbf{S}_{y,\pm} p_y$ (see Supplementary Note 2) with the anisotropic group velocities v_x and v_y, a new wave vector $\mathbf{p} = (p_x, p_y, 0)$ and the pseudospin vectors $\mathbf{S}_\pm = (\mathbf{S}_{x,\pm}, \mathbf{S}_{y,\pm}, \mathbf{S}_{z,\pm})$, which satisfies $[S_{m,\pm}, S_{n,\pm}] = i\varepsilon_{mnl} S_{l,\pm}$ with the Levi-Civita symbol ε_{mnl}. The expressions of these quantities are given in Supplementary Table 1, where $\mathbf{p} = \mathbf{Aq}$ with **A**, as a corresponding deformation operator similar to the manipulation of the in-plain strain[78]. Recently, searching for flat band has been particularly interesting, because the dispersionless state in the presence of Coulomb interactions can induce correlated quantum states, including ferromagnetism, superconductivity and fractional quantum Hall effect[79–82]. Recent experiments have shown that the localized flat band occurs in a photonic Lieb lattice that consists of an array of optical waveguides[83,84]. However, the flat band in real material has not been observed, since few 2D materials have the desired Lieb lattice. Here we predict the localized flat band that results from the destructive interference of electron hoppings rather than disorders or impurities by means of the light-engineered Lieb lattice in 2D MOFs.

Truncated Floquet Hamiltonian, Floquet half-metal and Floquet quantum spin Hall insulator. In the above sections, the zeroth static Floquet Hamiltonian predicts the light-induced topological phase transitions and the pseudospin-1 Dirac-Weyl fermions in 2D MOFs, but with the decrease of driving frequency ($t_1 < \omega < \Lambda$) the Floquet sidebands overlap such that the resonant absorptions or emissions of photons cannot be captured by the zeroth Floquet Hamiltonian. In this case, the Floquet Hamiltonian with infinite dimensions

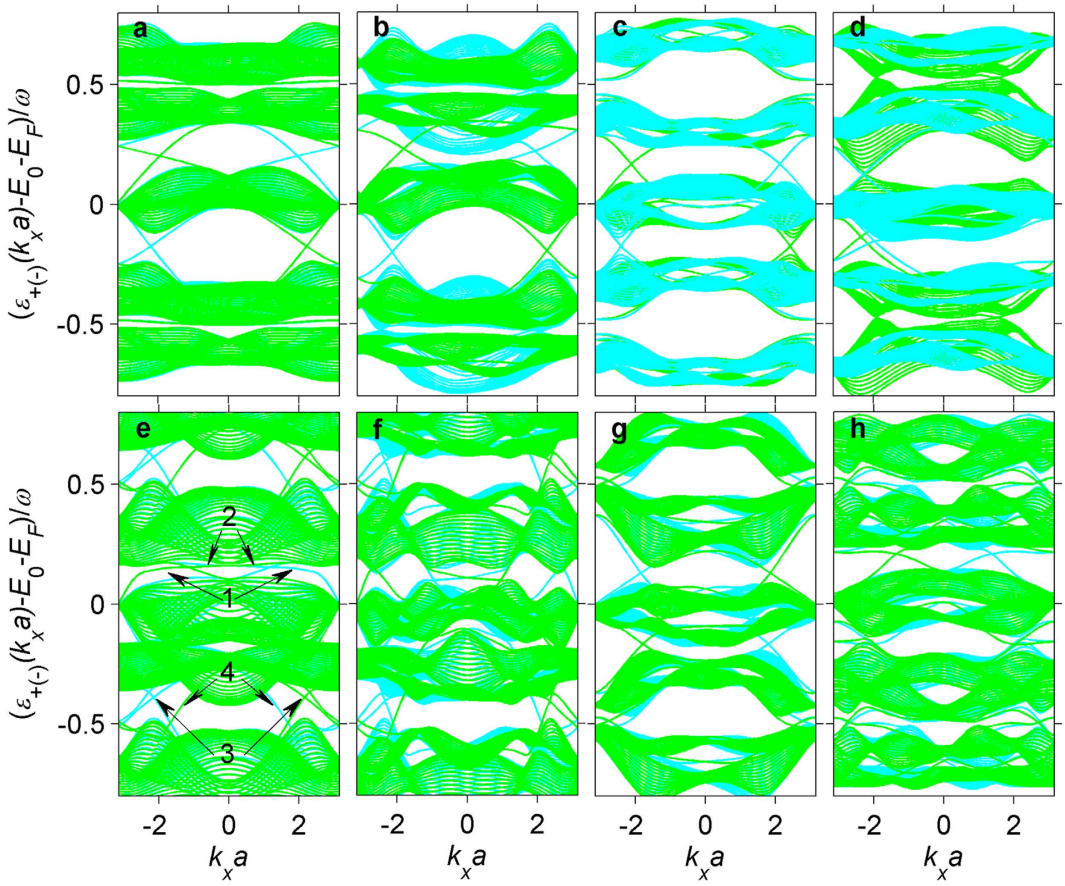

Figure 5. Quasienergy spectra of truncated Floquet Hamiltonian for light-irradiated $M_3C_{12}S_{12}$ on a cylindrical geometry. Quasienergy spectrum for linearly (**a**) and circularly (**b**) polarized light with $A_x a = 2.5$, $A_y a = 2.5$, and $\omega = 3t_1$. Quasienergy spectrum for linearly (**c**) and circularly (**d**) polarized light with $A_x a = 6.5$, $A_y a = 6.5$, and $\omega = 2t_1$. Quasienergy spectrum for linearly polarized light: (**e**) $A_x a = 1.5$, $A_y a = 1.5$, and $\omega = 2.4t_1$; (**f**) $A_x a = 0.5$, $A_y a = 2.5$, and $\omega = 2t_1$; (**g**) $A_x a = 6$, $A_y a = 0$, and $\omega = 2t_1$; and (**h**) $A_x a = 8$, $A_y a = 2$, and $\omega = 2t_1$. Here $E_0 = 0$, the spin-up and spin-down quasienergy spectra are denoted by green and cyan lines, respectively, and the electron densities for the edge states 1, 2, 3 and 4 in Fig. 5e are shown in Supplementary Fig. 2.

$(-\infty < m, n < +\infty)$ should be considered in principle. However, the Floquet indexes m and n can be truncated to a finite order M, because the FP substitution $\widetilde{f}_{i,j}^{M,M}$ vanishes with the Bessel function of the first kind $J_{n>M}(x) \sim 0$ (where M is a positive integer greater than x)[85] and makes the Floquet states $\phi_{n,m}$ decay rapidly if m and n are beyond the finite range M in frequency domain. The truncated Floquet Hamiltonian of 2D MOFs, with $3M \times 3M$ dimensions in the Sambe space[86], includes the resonant processes of few and multiple photons beyond the weak intensity limit, which only takes the single-photon absorption or emission into account. Based on the truncated Floquet Hamiltonian, we calculate the quasienergy spectra (Fig. 5) of $M_3C_{12}S_{12}$ irradiated by the on-resonant light with $\lambda_1 = 0.2t_1$, on the same cylindrical geometry as in Fig. 3. Unlike the harmonic driving of electric field always with the time-reversal symmetry[87], the on-resonant light driving keeps the time-reversal invariant for the linear polarization, *i.e.*, $\varepsilon_+(k_x a) = \varepsilon_-(-k_x a)$[88] but breaks the time-reversal symmetry for the circular polarization, *i.e.*, $\varepsilon_+(k_x a) \neq \varepsilon_-(-k_x a)$[14–19,25]. As a consequence, the on-resonant linearly polarized light only induces the dynamical gap near $\pm\omega/2$, and has few influences on the spin-polarized gapless helical edge states inside the two native bulk gaps of the undriven $M_3C_{12}S_{12}$ (Fig. 5a and c). However, the on-resonant circularly polarized light induces a dynamical gap for one spin but metals for the other spin (Fig. 5b and d), which results in the 100% spin-polarization, *i.e.*, the typical half-metallicity, owing to the broken time-reversal symmetry. The driven half-metal near the boundary $(\pm\omega/2)$ of the quasienergy Brillouin zone is without an analog in the undriven system, and hence is here named as Floquet half-metal. In addition, no matter the driving intensity is strong or weak, the Floquet half-metal can remain inside a limited frequency range $(\Lambda/2 < \omega < \Lambda)$ before the dynamical gap for both spins closes. Therefore, the Floquet half-metal is robust against the deviations of the optical parameters and the SOC intensity (see Supplementary Fig. 1). On the other hand, when the driving frequency of the linearly polarized light decreases further and becomes lower than $\Lambda/2$, some new gapless helical edge states protected by the time-reversal symmetry appear in the dynamical gap, which first closes and then reopens (Fig. 5e–h). In this case, $M_3C_{12}S_{12}$ is converted into the Floquet quantum spin Hall insulator[47,87] if the Fermi level is inside the dynamical gap. These new and initial gapless helical edge states exhibit well localizations at the two open

boundaries of the ribbon, and can coexist inside the same system with few couplings because of the big energy difference between each other (Supplementary Fig. 2).

Discussion

In this section, we first comment on the experimental feasibility to probe the predicted pseudospin-1 Dirac-Weyl fermions and the light-induced novel topological quantum phases in 2D MOFs. The Angle-resolved photoemission spectroscopy (ARPES) is a useful tool to map the electronic band dispersions of topological materials[5,6], by virtue of its important information on the kinetic energy and the emission angle of emitted photoelectrons. Recently, ARPES not only has been applied to acquire the Floquet-Bloch bands of TIs (Bi_2Se_3) irradiated by the monochromatic infra light with tunable intensity, frequency and polarization[19], but also has been used to distinguish the Floquet-Bloch states from the Volkov states, *i.e.*, the photon-dressed free-electron states near the surface of TIs[89]. Besides, both of the occupied and unoccupied energy bands near and far away the Fermi level can be resolved by the one-photon and two-photon ARPES[90]. Other methods are also proposed to check the Floquet-Bloch states in Floquet TIs. For instance, the mean orbital magnetization, as a result of the Floquet topological edge currents, has been suggested as a hallmark signature of the light-induced Floquet topological quantum states[91]. In addition, various 2D MOFs have been synthesized in recent experiments by the bottom-up method[54–57], and the Fermi level of the single-atom-layer material can be well controlled by the back gate[92]. Therefore, we believe that the predicted light-induced pseudospin-1 Dirac-Weyl energy spectrum and the Floquet-Bloch topological band dispersions in 2D MOFs can be probed by a combination of the ARPES and the gate-controllable Fermi level.

Next, we summarize our results and present an outlook for future investigations. We explore the effects of light on the quantum phases and the topological properties of 2D MOFs with kagome lattice ($M_3C_{12}S_{12}$) within the framework of the off-resonant and on-resonant Floquet-Bloch physics. It is shown that unusual Floquet quantum states can be engineered in the same 2D MOFs by virtue of highly tunable parameters of light. For instance, the claimed nontrivial Floquet quantum spin Hall states in the driven 2D lattice system[47] as well as the cold atom system[87] and the theoretically predictable[70–74] and experimentally observable[83,84] pseudospin-1 Dirac-Weyl fermions with flat bands in the photonic Lieb lattice are realized in the light-irradiated 2D MOFs. Moreover, we also observe that a new Floquet half-metallic state can be engineered in 2D MOFs by the on-resonant circularly polarized light that breaks the time-reversal symmetry. These results not only facilitate the developments of Floquet-Bloch physics in condensed matter, but also open a new path towards light-controlled spintronics and optoelectronics based on 2D MOFs. On the other hand, as a starting point, light-irradiated 2D MOFs also raise many interesting subjects, which deserve further explorations in future. Firstly, in the presence of interactions, periodically driven system exhibits novel Floquet many-body states[28,93–97], such as the fractional Chern insulator states[28], which generically support the fractional quantum Hall states[79–82]. Our results has demonstrated that the expected topological flat band with a large flatness ratio, which is a crucial condition for the occurrence of the fractional quantum Hall effect[79–82], can be engineered by the off-resonant light in 2D MOFs (see Figs 3a,d and 4). In addition, the strong electronic correlations can be introduced by choosing the different combinations of metal ions and organic ligands. Therefore, the light-irradiated 2D MOFs may offer theoretical and experimental platforms to realize the fractional Chern insulator states in real materials. Secondly, a spatial modulation of light allows for remarkably tuning the Floquet topological properties of semiconductor quantum wells[22] and the surface states of three-dimensional topological insulators[98]. However, how about the situation in 2D crystal materials, *i.e.*, the 2D MOFs with the kagome lattice under the spatially nonuniform irradiations? Thirdly, the temperature-dependent 2D topological phases have been characterized by the Uhlmann geometric phase[99,100]. It remains unclear, however, how to characterize the Floquet topological phases at finite temperature in 2D MOFs and other materials. Finally, after the above question of the temperature-dependent Floquet topological phases is addressed, and the experimental measurements on the Floquet topological quantum states in light-irradiated 2D materials are completed, Further experiments are required to explore the coupling mechanism between the Floquet TIs and the external reservoirs[52], the electron occupations of the nonequilibrium Floquet states[101,102] and the dc Hall conductance of the driven Floquet TIs[48].

Methods

Tight-binding (TB) model on the kagome lattice in 2D MOFs. The equivalent single-orbital TB Hamiltonian of the kagome lattice[79,103], describing the interactions between the π orbitals of the ligands and the d orbitals of the metal ions in 2D MOFs[58–66], should in principle involve the nearest-neighbor and next-nearest-neighbor interactions, and can be written as

$$\begin{aligned} H_0 &= E_0\sum_{i,\alpha} c_{i\alpha}^{\dagger}c_{i\alpha} - t_1\sum_{\langle i,j\rangle,\alpha} c_{i\alpha}^{\dagger}c_{j\alpha} + i\frac{8\lambda_1}{\sqrt{3}}\sum_{\langle i,j\rangle,\alpha,\beta}(\mathbf{d}_{kj}\times\mathbf{d}_{ik})\cdot\mathbf{S}_{\alpha\beta}c_{i\alpha}^{\dagger}c_{j\beta} \\ &\quad - t_2\sum_{\langle\langle i,j\rangle\rangle,\alpha} c_{i\alpha}^{\dagger}c_{j\alpha} + i\frac{8\lambda_2}{3\sqrt{3}}\sum_{\langle\langle i,j\rangle\rangle,\alpha,\beta}(\mathbf{D}_{kj}\times\mathbf{D}_{ik})\cdot\mathbf{S}_{\alpha\beta}c_{i\alpha}^{\dagger}c_{j\beta} \end{aligned} \quad (3)$$

Here the first term is the on-site energy. The second and third terms are the nearest-neighbor (denoted by $\langle i, j\rangle$) hopping and intrinsic SOC with energy parameters t_1 and λ_1, respectively. The last two terms are the next-nearest-neighbor (denoted by $\langle\langle i, j\rangle\rangle$) hopping and intrinsic SOC with energy parameters t_2 and λ_2, respectively. $\mathbf{S}$ is the spin Pauli matrix. $\mathbf{d}_{kj}$ and $\mathbf{D}_{kj}$ are the nearest-neighbor and next-nearest-neighbor vectors pointing from site $\mathbf{r}_j$ to $\mathbf{r}_k$, respectively (Fig. 1b). The factors $8/\sqrt{3}$ and $8/3\sqrt{3}$ correspondingly ensure the vectors $\mathbf{d}_{kj}$ and $\mathbf{D}_{kj}$ normalized to the unite vectors, similar to that in graphene[75] or silicene[26]. In fact, owing to $t_1 \gg t_2$ and $\lambda_1 \gg \lambda_2$[59–66],

the nearest-neighbor interactions are the main components, and hence the quite weak next-nearest-neighbor interactions are usually not considered in 2D MOFs[59–61].

Floquet-Bloch theory in the light-irradiated $M_3C_{12}S_{12}$. In the presence of monochromatic infrared light with its spatially slowly varying electromagnetic potential $\mathbf{A}(t) = (A_x \sin(\omega t), A_y \sin(\omega t + \phi), 0)$ (Fig. 1a), the time-dependent TB Hamiltonian as a result of the Peierls substitution has the following form:

$$\begin{aligned} H(t) &= E_0 \sum_{i,\alpha} c_{i\alpha}^{\dagger} c_{i\alpha} - t_1 \sum_{\langle i,j\rangle,\alpha} e^{i\int_i^j \mathbf{A}(t)\cdot d\mathbf{r}} c_{i\alpha}^{\dagger} c_{j\alpha} \\ &\quad + i\frac{8\lambda_1}{\sqrt{3}} \sum_{\langle i,j\rangle,\alpha,\beta} e^{i\int_i^j \mathbf{A}(t)\cdot d\mathbf{r}} (\mathbf{d}_{kj} \times \mathbf{d}_{ik}) \cdot \mathbf{S}_{\alpha\beta} c_{i\alpha}^{\dagger} c_{j\beta}. \end{aligned} \tag{4}$$

We further perform the following Fourier transforms[20]

$$\begin{aligned} c_{\mathbf{k},\alpha}^{\dagger} &= \frac{1}{\sqrt{N}} \sum_{j=1}^{N} (c_{A,j\alpha}^{\dagger} \;\; c_{B,j\alpha}^{\dagger} \;\; c_{C,j\alpha}^{\dagger}) e^{i\mathbf{k}\cdot\mathbf{r}_j} \\ c_{\mathbf{k},\alpha} &= \frac{1}{\sqrt{N}} \sum_{j=1}^{N} (c_{A,j\alpha} \;\; c_{B,j\alpha} \;\; c_{C,j\alpha})^{\mathbf{T}} e^{-i\mathbf{k}\cdot\mathbf{r}_j} \end{aligned}, \tag{5}$$

where N is the number of sites with periodic boundary conditions, $\mathbf{T}$ denotes the transpose operation, $\mathbf{k}$ is the wave vector defined in the Brillouin zone, and A, B and C are the three sublattices of a unit cell in kagome lattice (Fig. 1b). Then we can rewrite the time-dependent Hamiltonian in momentum space as

$$H(t) = \sum_{\mathbf{k}} (c_{\mathbf{k}\uparrow}^{\dagger} \;\; c_{\mathbf{k}\downarrow}^{\dagger}) H(\mathbf{k}, t) \begin{pmatrix} c_{\mathbf{k}\uparrow} \\ c_{\mathbf{k}\downarrow} \end{pmatrix}, \tag{6}$$

where $c_{\mathbf{k}\alpha}^{\dagger} = \left(c_{A,\mathbf{k}\alpha}^{\dagger} \;\; c_{B,\mathbf{k}\alpha}^{\dagger} \;\; c_{C,\mathbf{k}\alpha}^{\dagger}\right)$ and $c_{\mathbf{k}} = (c_{A,\mathbf{k}\alpha} \;\; c_{B,\mathbf{k}\alpha} \;\; c_{C,\mathbf{k}\alpha})^{\mathbf{T}}$ are the creation/annihilation operators for an electron with the spin α ($\uparrow$ and $\downarrow$ denote spin up and down, respectively) in momentum space. Due to $[\mathbf{S}_z, H(t)] = 0$, the 6×6 matrix $H(\mathbf{k}, t)$ can be decoupled into two 3×3 spin-dependent Hamiltonians:

$$\begin{aligned} H_{\pm}(\mathbf{k}, t) &= E_0 \mathbf{I} - t_1 \begin{bmatrix} 0 & f_1(t) + f_1^*(t) e^{ik_2} & f_3(t) + f_3^*(t) e^{ik_3} \\ f_1^*(t) + f_1(t) e^{-ik_2} & 0 & f_2(t) + f_2^*(t) e^{-ik_1} \\ f_3^*(t) + f_3(t) e^{-ik_3} & f_2^*(t) + f_2(t) e^{ik_1} & 0 \end{bmatrix} \\ &\quad \pm i\lambda_1 \begin{bmatrix} 0 & f_1(t) + f_1^*(t) e^{ik_2} & -f_3(t) - f_3^*(t) e^{ik_3} \\ -f_1^*(t) - f_1(t) e^{-ik_2} & 0 & f_2(t) + f_2^*(t) e^{-ik_1} \\ f_3^*(t) + f_3(t) e^{-ik_3} & -f_2^*(t) - f_2(t) e^{ik_1} & 0 \end{bmatrix} \end{aligned}, \tag{7}$$

where $k_i = \mathbf{k} \cdot \mathbf{a}_i$, $\mathbf{I}$ is the 3×3 unite matrix, $+(-)$ refers to spin-up (spin-down), and the time-dependent Peierls substitutions are

$$\begin{aligned} f_1(t) &= e^{-iA_x a \sin(\omega t)/4} e^{-i\sqrt{3}A_y a \sin(\omega t + \phi)/4} \\ f_2(t) &= e^{iA_x a \sin(\omega t)/2} \\ f_3(t) &= e^{iA_x a \sin(\omega t)/4} e^{-i\sqrt{3}A_y a \sin(\omega t + \phi)/4} \end{aligned}. \tag{8}$$

Employing the Floquet theorem, we can write Floquet-Bloch ansatz as

$$|\psi_{\pm}(\mathbf{k}, t)\rangle = e^{-i\varepsilon_{\pm}(\mathbf{k})t} |\Phi_{\pm}(\mathbf{k}, t)\rangle = e^{-i\varepsilon_{\pm}(\mathbf{k})t} |\Phi_{\pm}(\mathbf{k}, t + T)\rangle = e^{-i\varepsilon_{\pm}(\mathbf{k})t} \sum_{m=-\infty}^{+\infty} |\Phi_{\pm}(\mathbf{k})\rangle e^{im\omega t}, \tag{9}$$

with the period T, the spin-dependent quasienergy $\varepsilon_{\pm}(\mathbf{k})$ and the Floquet-Bloch states $|\Phi_{\pm}(\mathbf{k}, t)\rangle$. The Floquet operator $H_{F,\pm}(\mathbf{k}, t) = H_{\pm}(\mathbf{k}, t) - i\hat{\partial}_t$ yields the time-independent Floquet energy eigenvalue equation in the Sambe space as

$$\sum_{n=-\infty}^{+\infty} [\widetilde{H}_{\pm}^{m,n}(\mathbf{k}) + n\omega\delta_{mn}] |\Phi_{\pm}(\mathbf{k})\rangle = \varepsilon_{\pm}(\mathbf{k}) |\Phi_{\pm}(\mathbf{k})\rangle, \tag{10}$$

where the time-independent Hamiltonian $\widetilde{H}_{\pm}^{m,n}(\mathbf{k})$ with the Floquet indexes (m, n) includes the emissions or absorptions of q photons ($q = m - n$) and takes the form:

$$\widetilde{H}_{\pm}^{m,n}(\mathbf{k}) = \frac{1}{T} \int_0^T e^{-i(m-n)\omega t} H_{\pm}(\mathbf{k}, t) dt = \frac{1}{T} \int_0^T e^{-iq\omega t} H_{\pm}(\mathbf{k}, t) dt. \tag{11}$$

Substituting equations (6) and (7) into equation (10), we find that $\widetilde{H}_{\pm}^{m,n}(\mathbf{k})$ takes the same forms as the undriven static Hamiltonian but with new hopping integrals and SOC strengths modified by the time-averaged Peierls (Floquet-Peierls) substitutions:

$$\widetilde{f}_{i,j}^{m,n} = \frac{1}{T}\int_0^T e^{-i(m-n)\omega t} f_{i,j}(t)\,dt. \tag{12}$$

Spin chern number and spin Hall conductance. The absence of Rashba SOC in $M_3C_{12}S_{12}$ conserves the spin rotational symmetry, and hence the spin-dependent chern number $C_{\pm}^{i}$ of the energy band i can be directly calculated using the Kubo formula

$$C_{\pm}^{i} = -\frac{1}{2\pi}\int_{BZ} d^2\vec{k}\,\mathrm{Im}\sum_{i\neq j}\frac{\langle i_{\pm}|\hat{v}_{x,\pm}|j_{\pm}\rangle\langle j_{\pm}|\hat{v}_{y,\pm}|i_{\pm}\rangle - \langle i_{\pm}|\hat{v}_{y,\pm}|j_{\pm}\rangle\langle j_{\pm}|\hat{v}_{x,\pm}|i_{\pm}\rangle}{(\varepsilon_{\pm}^{i} - \varepsilon_{\pm}^{j})^2}, \tag{13}$$

where $+(-)$ refers to spin-up (spin-down), $\varepsilon_{\pm}^{i}$ ($\varepsilon_{\pm}^{j}$) is the spin-dependent eigenvalue of the energy band i (j), and $\hat{v}_{x(y)}$ is the velocity operator. The chern number of band i is $C^i = C_{+}^{i} + C_{-}^{i}$ and the spin chern number of band i is $C_s^i = (C_{+}^{i} - C_{-}^{i})/2$. From the spin Chern number, we can further write the spin Hall conductance as $\sigma_{xy}^{s}(E) = (e/2\pi)\sum_{\varepsilon_{\pm}^{i}<E} C_s^i$.

References

1. Žutić, I., Fabian, J. & Das Sarma, S. Spintronics: Fundamentals and applications. *Rev. Mod. Phys.* **76,** 323–410 (2004).
2. Castro Neto, A. H., Guinea, F., Peres, N. M. R., Novoselov, K. S. & Geim, A. K. The electronic properties of graphene. *Rev. Mod. Phys.* **81,** 109–162 (2009).
3. Rycerz, A., Tworzydlo, J. & Beenakker, C. W. J. Valley filter and valley valve in graphene. *Nature Phys.* **3,** 172–175 (2007).
4. Xu, X., Yao, W., Xiao, D. & Heinz, T. F. Spin and pseudospins in layered transition metal dichalcogenides. *Nature Phys.* **10,** 343–350 (2014).
5. Hasan, M. Z. & Kane, C. L. Topological insulators. *Rev. Mod. Phys.* **82,** 3045–3067 (2010).
6. Qi, X. L. & Zhang, S. C. Topological insulators and superconductors. *Rev. Mod. Phys.* **83,** 1057–1110 (2011).
7. Wan, X., Turner, A. M., Vishwanath, A. & Savrasov, S. Y. Topological semimetal and Fermi-arc surface states in the electronic structure of pyrochlore iridates. *Phys. Rev. B* **83,** 205101 (2011).
8. Xu, G., Weng, H., Wang, Z., Dai, X. & Fang, Z. Chern semimetal and the quantized anomalous Hall effect in $HgCr_2Se_4$. *Phys. Rev. Lett.* **107,** 186806 (2011).
9. Burkov, A. A. & Balents, L. Weyl semimetal in a topological insulator multilayer. *Phys. Rev. Lett.* **107,** 127205 (2011).
10. Young, S. M. *et al.* Dirac semimetal in three dimensions. *Phys. Rev. Lett.* **108,** 140405 (2012).
11. Wang, Z. J. *et al.* Dirac semimetal and topological phase transitions in A_3Bi (A = Na, K, Rb). *Phys. Rev. B* **85,** 195320 (2012).
12. Oka, T. & Aoki, H. Photovoltaic Hall effect in graphene. *Phys. Rev. B* **79,** 081406 (2009).
13. Kitagawa, T., Berg, E., Rudner, M. & Demler, E. Topological characterization of periodically driven quantum systems. *Phys. Rev. B* **82,** 235114 (2010).
14. Inoue, J. I. & Tanaka, A. Photoinduced transition between conventional and topological insulators in two-dimensional electronic systems. *Phys. Rev. Lett.* **105,** 017401 (2010).
15. Lindner, N. H., Refael, G. & Galitski, V. Floquet topological insulator in semiconductor quantum wells. *Nat. Phys.* **7,** 490–495 (2011).
16. Gu, Z., Fertig, H. A., Arovas, D. P. & Auerbach, A. Floquet spectrum and transport through an irradiated graphene ribbon. *Phys. Rev. Lett.* **107,** 216601 (2011).
17. Kitagawa, T., Oka, T., Brataas, A., Fu, L. & Demler, E. Transport properties of nonequilibrium systems under the application of light: Photoinduced quantum Hall insulators without Landau levels. *Phys. Rev. B* **84,** 235108 (2011).
18. Dora, B., Cayssol, J., Simon, F. & Moessner, R. Optically engineering the topological properties of a spin Hall insulator. *Phys. Rev. Lett.* **108,** 056602 (2012).
19. Wang, Y. H., Steinberg, H., Jarillo-Herrero, P. & Gedik, N. Observation of Floquet-Bloch states on the surface of a topological insulator. *Science* **342,** 453–457 (2013).
20. Gómez-León, A. & Platero, G. Floquet-Bloch theory and topology in periodically driven lattices. *Phys. Rev. Lett.* **110,** 200403 (2013).
21. Fregoso, B. M., Wang, Y. H., Gedik, N. & Galitski, V. Driven electronic states at the surface of a topological insulator. *Phys. Rev. B* **88,** 155129 (2013).
22. Katan, Y. T. & Podolsky, D. Modulated Floquet topological insulators. *Phys. Rev. Lett.* **110,** 016802 (2013).
23. Delplace, P., Gómez-León, Á. & Platero, G. Merging of Dirac points and Floquet topological transitions in ac-driven graphene. *Phys. Rev. B* **88,** 245422 (2013).
24. Lindner, N. H., Bergman, D. L., Refael, G. & Galitski, V. Topological Floquet spectrum in three dimensions via a two-photon resonance. *Phys. Rev. B* **87,** 235131 (2013).
25. Usaj, G., Perez-Piskunow, P. M., Torres, L. F. & Balseiro, C. A. Irradiated graphene as a tunable Floquet topological insulator. *Phys. Rev. B* **90,** 115423 (2014).
26. Ezawa, M. Photoinduced topological phase transition and a single Dirac-cone state in silicene. *Phys. Rev. Lett.* **110,** 026603 (2013).
27. Quelle, A. & Smith, C. M. Dynamical competition between quantum Hall and quantum spin Hall effects. *Phys. Rev. B* **90,** 195137 (2014).
28. Grushin, A. G., Gómez-León, Á. & Neupert, T. Floquet fractional Chern insulators. *Phys. Rev. Lett.* **112,** 156801 (2014).
29. Sentef, M. A. *et al.* Theory of Floquet band formation and local pseudospin textures in pump-probe photoemission of graphene. *Nat. Commun.* **6,** 7047 (2015).
30. D'Alessio, L. & Rigol, M. Dynamical preparation of Floquet Chern insulators. *Nat. Commun.* **6,** 8336 (2015).
31. Wang, R., Wang, B., Shen, R., Sheng, L. & Xing, D. Y. Floquet Weyl semimetal induced by off-resonant light. *EPL* **105,** 17004 (2014).
32. Zou, J. Y. & Liu, B. G. Floquet Weyl fermions in three-dimensional stacked graphene systems irradiated by circularly polarized light. *Phys. Rev. B* **93,** 205435 (2016).
33. Yan, Z. & Wang, Z. Tunable Weyl Semimetals in Periodically Driven Nodal Line Semimetals. *Phys. Rev. Lett.* **117,** 087402 (2016).
34. Wang, H., Zhou, L. & Chong, Y. D. Floquet Weyl phases in a three-dimensional network model. *Phys. Rev. B* **93,** 144114 (2016).
35. Zhou, L., Chen, C. & Gong, J. Floquet semimetal with Floquet-band holonomy. *Phys. Rev. B* **94,** 075443 (2016).
36. Chan, C. K., Oh, Y. T., Han, J. H. & Lee, P. A. Type-II Weyl cone transitions in driven semimetals. *Phys. Rev. B* **94,** 121106 (2016).

37. Jiang, L. *et al.* Majorana fermions in equilibrium and driven cold atom quantum wires. *Phys. Rev. Lett.* **106,** 220402 (2011).
38. Kitagawa, T. *et al.* Observation of topologically protected bound states in photonic quantum walks. *Nat. Commun.* **3,** 882 (2012).
39. Rechtsman, M. C. *et al.* Photonic Floquet topological insulators. *Nature* **496,** 196 (2013).
40. Zheng, W. & Zhai, H. Floquet topological states in shaking optical lattices. *Phys. Rev. A* **89,** 061603 (2014).
41. Goldman, N. & Dalibard, J. Periodically driven quantum systems: effective Hamiltonians and engineered gauge fields. *Phys. Rev. X* **4,** 031027 (2014).
42. Titum, P., Berg, E., Rudner, M. S., Refael, G. & Lindner, N. H. Anomalous Floquet-Anderson Insulator as a Nonadiabatic Quantized Charge Pump. *Phys. Rev. X* **6,** 021013 (2016).
43. Rudner, M. S., Lindner, N. H., Berg, E. & Levin, M. Anomalous Edge States and the Bulk-Edge Correspondence for Periodically Driven Two-Dimensional Systems. *Phys. Rev. X* **3,** 031005 (2013).
44. Asbóth, J. K., Tarasinski, B. & Delplace, P. Chiral symmetry and bulk-boundary correspondence in periodically driven one-dimensional systems. *Phys. Rev. B* **90,** 125143 (2014).
45. Ho, D. Y. & Gong, J. Topological effects in chiral symmetric driven systems. *Phys. Rev. B* **90,** 195419 (2014).
46. Zhou, Z., Satija, I. I. & Zhao, E. Floquet edge states in a harmonically driven integer quantum Hall system. *Phys. Rev. B* **90,** 205108 (2014).
47. Carpentier, D., Delplace, P., Fruchart, M. & Gawędzki, K. Topological index for periodically driven time-reversal invariant 2D systems. *Phys. Rev. Lett.* **114,** 106806 (2015).
48. Torres, L. F., Perez-Piskunow, P. M., Balseiro, C. A. & Usaj, G. Multiterminal conductance of a Floquet topological insulator. *Phys. Rev. Lett.* **113,** 266801 (2014).
49. Kundu, A. & Seradjeh, B. Transport signatures of Floquet Majorana fermions in driven topological superconductors. *Phys. Rev. Lett.* **111,** 136402 (2013).
50. Li, Y., Kundu, A., Zhong, F. & Seradjeh, B. Tunable Floquet Majorana fermions in driven coupled quantum dots. *Phys. Rev. B* **90,** 121401 (2014).
51. Wang, P., Sun, Q. F. & Xie, X. C. Transport properties of Floquet topological superconductors at the transition from the topological phase to the Anderson localized phase. *Phys. Rev. B* **90,** 155407 (2014).
52. Dehghani, H., Oka, T. & Mitra, A. Out-of-equilibrium electrons and the Hall conductance of a Floquet topological insulator. *Phys. Rev. B* **91,** 155422 (2015).
53. Farrell, A. & Pereg-Barnea, T. Edge-state transport in Floquet topological insulators. *Phys. Rev. B* **93,** 045121 (2016).
54. Kambe, T. *et al.* Redox control and high conductivity of nickel bis(dithiolene) complexp-nanosheet: a potential organic two-dimensional topological insulator. *J. Am. Chem. Soc.* **136,** 14357–14360 (2014).
55. Sheberla, D. *et al.* High electrical conductivity in Ni_3(2,3,6,7,10,11-hexaiminotriphenylene)$_2$, a semiconducting metal-organic graphene analogue. *J. Am. Chem. Soc.* **136,** 8859–8862 (2014).
56. Huang, X. *et al.* A two-dimensional π-d conjugated coordination polymer with extremely high electrical conductivity and ambipolar transport behaviour. *Nat. Commun.* **6,** 7408 (2015).
57. Dong, R. *et al.* Large-Area, Free-Standing, Two-Dimensional Supramolecular Polymer Single-Layer Sheets for Highly Efficient Electrocatalytic Hydrogen Evolution. *Angew. Chem. Int. Ed.* **54,** 12058–12063 (2015).
58. Maeda, H., Sakamoto, R. & Nishihara, H. Coordination Programming of Two-Dimensional Metal Complex Frameworks. *Langmuir* **32,** 2527–2538 (2016).
59. Wang, Z. F., Liu, Z. & Liu, F. Organic topological insulators in organometallic lattices. *Nat. Commun.* **4,** 1471 (2013).
60. Wang, Z. F., Su, N. & Liu, F. Prediction of a two-dimensional organic topological insulator. *Nano Lett.* **13,** 2842–2845 (2013).
61. Zhao, B., Zhang, J., Feng, W., Yao, Y. & Yang, Z. Quantum spin Hall and Z_2 metallic states in an organic material. *Phys. Rev. B* **90,** 201403 (2014).
62. Zhou, Q. *et al.* Topological insulators based on 2D shape-persistent organic ligand complexes. *Nanoscale* **7,** 727–735 (2015).
63. Yamada, M., Soejima, T., Tsuji, N., Hirai, D., Dincă, M. & Aoki, H. First-Principles Design of a Half-Filled Flat Band of the Kagome Lattice in Two-Dimensional Metal-Organic Frameworks. *Phys. Rev. B* **94,** 081102(R) (2015).
64. Zhang, X., Wang, Z., Zhao, M. & Liu, F. Tunable topological states in electron-doped HTT-Pt. *Phys. Rev. B* **93,** 165401 (2016).
65. Dong, L., Kim, Y., Er, D., Rappe, A. M. & Shenoy, V. B. Two-Dimensional π-Conjugated Covalent-Organic Frameworks as Quantum Anomalous Hall Topological Insulators. *Phys. Rev. Lett.* **116,** 096601 (2016).
66. Kim, H. J., Li, C., Feng, J., Cho, J. H. & Zhang, Z. Competing magnetic orderings and tunable topological states in two-dimensional hexagonal organometallic lattices. *Phys. Rev. B* **93,** 041404 (2016).
67. Adjizian, J. J. *et al.* Dirac Cones in two-dimensional conjugated polymer networks. *Nat. Commun.* **5,** 5842 (2014).
68. Zhao, M., Wang, A. & Zhang, X. Half-metallicity of a kagome spin lattice: the case of a manganese bis-dithiolene monolayer. *Nanoscale* **5,** 10404–10408 (2013).
69. Campbell, M. G., Liu, S. F., Swager, T. M. & Dincă, M. Chemiresistive Sensor Arrays from Conductive 2D Metal-Organic Frameworks. *J. Am. Chem. Soc.* **137,** 13780–13783 (2015).
70. Bercioux, D., Urban, D. F., Grabert, H. & Häusler, W. Massless Dirac-Weyl fermions in a T_3 optical lattice. *Phys. Rev. A* **80,** 063603 (2009).
71. Shen, R., Shao, L. B., Wang, B. & Xing, D. Y. Single Dirac cone with a flat band touching on line-centered-square optical lattices. *Phys. Rev. B* **81,** 041410 (2010).
72. Green, D., Santos, L. & Chamon, C. Isolated flat bands and spin-1 conical bands in two-dimensional lattices. *Phys. Rev. B* **82,** 075104 (2010).
73. Lan, Z., Goldman, N., Bermudez, A., Lu, W. & Öhberg, P. Dirac-Weyl fermions with arbitrary spin in two-dimensional optical superlattices. *Phys. Rev. B* **84,** 165115 (2011).
74. Dóra, B., Kailasvuori, J. & Moessner, R. Lattice generalization of the Dirac equation to general spin and the role of the flat band. *Phys. Rev. B* **84,** 195422 (2011).
75. Sheng, D. N., Weng, Z. Y., Sheng, L. & Haldane, F. D. M. Quantum spin-Hall effect and topologically invariant Chern numbers. *Phys. Rev. Lett.* **97,** 036808 (2006).
76. Prodan, E. Robustness of the spin-Chern number. *Phys. Rev. B* **80,** 125327 (2009).
77. Kane, C. L. & Mele, E. J. Z_2 topological order and the quantum spin Hall effect. *Phys. Rev. Lett.* **95,** 146802 (2005).
78. Wang, B., Wang, Y. & Liu, Y. Generalized Hamiltonian for a graphene subjected to arbitrary in-plane strains. *Funct. Mater. Lett.* **08,** 1530001 (2015).
79. Tang, E., Mei, J. W. & Wen, X. G. High-temperature fractional quantum Hall states. *Phys. Rev. Lett.* **106,** 236802 (2011).
80. Neupert, T., Santos, L., Chamon, C. & Mudry, C. Fractional quantum Hall states at zero magnetic field. *Phys. Rev. Lett.* **106,** 236804 (2011).
81. Sun, K., Gu, Z., Katsura, H. & Sarma, S. D. Nearly flatbands with nontrivial topology. *Phys. Rev. Lett.* **106,** 236803 (2011).
82. Wang, Y. F., Gu, Z. C., Gong, C. D. & Sheng, D. N. Fractional quantum Hall effect of hard-core bosons in topological flat bands. *Phys. Rev. Lett.* **107,** 146803 (2011).
83. Vicencio, R. A. *et al.* Observation of localized states in Lieb photonic lattices. *Phys. Rev. Lett.* **114,** 245503 (2015).
84. Mukherjee, S. *et al.* Observation of a localized flat-band state in a photonic Lieb lattice. *Phys. Rev. Lett.* **114,** 245504 (2015).
85. Olver, F. W., Lozier, D. W., Boisvert, R. F. & Clark, C. W. *NIST Handbook of Mathematical Functions Hardback and CD-ROM* (Cambridge Univ. Press, New York, 2010).

86. Sambe, H. Steady states and quasienergies of a quantum-mechanical system in an oscillating field. *Phys. Rev. A* **7,** 2203 (1973).
87. Yan, Z., Li, B., Yang, X. & Wan, S. A General Time-Periodic Driving Approach to Realize Topological Phases in Cold Atomic Systems. *Sci. Rep*. **5,** 16197 (2015).
88. Pi, S. T. & Savrasov, S. Polarization induced Z_2 and Chern topological phases in a periodically driving field. *Sci. Rep*. **6,** 22993 (2016).
89. Mahmood, F. *et al.* Selective scattering between Floquet-Bloch and Volkov states in a topological insulator. *Nat. Phys*. **12,** 306–310 (2016).
90. Sobota, J. A. *et al.* Direct optical coupling to an unoccupied Dirac surface state in the topological insulator Bi_2 Se_3. *Phys. Rev. Lett.* **111,** 136802 (2013).
91. Dahlhaus, J. P., Fregoso, B. M. & Moore, J. E. Magnetization signatures of light-induced quantum Hall edge states. *Phys. Rev. Lett.* **114,** 246802 (2015).
92. Novoselov, K. S. *et al.* Electric field effect in atomically thin carbon films. *science* **306,** 666–669 (2004).
93. Mikami, T. *et al.* Brillouin-Wigner theory for high-frequency expansion in periodically driven systems: Application to Floquet topological insulators. *Phys. Rev. B* **93,** 144307 (2016).
94. Klinovaja, J., Stano, P. & Loss, D. Topological Floquet Phases in Driven Coupled Rashba Nanowires. *Phys. Rev. Lett.* **116,** 176401 (2016).
95. Abanin, D. A., De Roeck, W. & Huveneers, F. Exponentially slow heating in periodically driven many-body systems. *Phys. Rev. Lett.* **115,** 256803 (2015).
96. Iadecola, T., Santos, L. H. & Chamon, C. Stroboscopic symmetry-protected topological phases. *Phys. Rev. B* **92,** 125107 (2015).
97. von Keyserlingk, C. W. & Sondhi, S. L. Phase structure of one-dimensional interacting Floquet systems. I. Abelian symmetry-protected topological phases. *Phys. Rev. B* **93,** 245145 (2016).
98. Calvo, H. L., Torres, L. F., Perez-Piskunow, P. M., Balseiro, C. A. & Usaj, G. Floquet interface states in illuminated three-dimensional topological insulators. *Phys. Rev. B* **91,** 241404 (2015).
99. Viyuela, O., Rivas, A. & Martin-Delgado, M. A. Uhlmann phase as a topological measure for one-dimensional fermion systems. *Phys. Rev. Lett.* **112,** 130401 (2014).
100. Huang, Z. & Arovas, D. P. Topological indices for open and thermal systems via Uhlmann's phase. *Phys. Rev. Lett.* **113,** 076407 (2014).
101. Liu, D. E. Classification of the Floquet statistical distribution for time-periodic open systems. *Phys. Rev. B* **91,** 144301 (2015).
102. Iadecola, T., Neupert, T. & Chamon, C. Occupation of topological Floquet bands in open systems. *Phys. Rev. B* **91,** 235133 (2015).
103. Guo, H. M. & Franz, M. Topological insulator on the kagome lattice. *Phys. Rev. B* **80,** 113102 (2009).

Acknowledgements

This work was supported financially by National Natural Science Foundation of China (Grant Nos 10572155, 11472313, 11502308 and 11572355) and Guangdong Natural Science Foundation of China (Grant No. 2016A030310205).

Author Contributions

Y.H.W. and B.W. conceived the research. Y.H.W. developed the computer codes and performed the calculations and analysis. Y.H.W. and B.W. wrote the manuscript. Y.H.W., Y.L. and B.W. discussed the results and commented on the manuscript.

Additional Information

Supplementary information accompanies this paper at http://www.nature.com/srep

Competing financial interests: The authors declare no competing financial interests.

How to cite this article: Wang, Y. *et al.* Effects of light on quantum phases and topological properties of two-dimensional Metal-organic frameworks. *Sci. Rep.* **7**, 41644; doi: 10.1038/srep41644 (2017).

Publisher's note: Springer Nature remains neutral with regard to jurisdictional claims in published maps and institutional affiliations.